PCCP

PAPER

View Article Online
View Journal | View Issue

Cite this: *Phys. Chem. Chem. Phys.*, 2025, **27**, 18459

Mechanistic insights into glycosylation-driven structural rearrangements in human aquaporin 1

Keisuke Saito, *[ab] Yasuhiro Kajihara *[c] and Hiroshi Ishikita *[ab]

The asparagine-linked glycosylation site of the extended extracellular loop connecting transmembrane helices 1 and 2 has been identified in human aquaporin 1 (AQP1), though its functional significance remains unclear. Here, we investigate AQP1 glycosylated at Asn42 and Asn205, using molecular dynamics simulations. In glycosylated AQP1, fluctuation of the protein backbone groups surrounding the linker Asn42 in the extended extracellular loop 1–2 is significantly suppressed compared to non-glycosylated AQP1. The heavily hydrated glycan at Asn42 stretches the extracellular loop, which in turn induces conformational changes that propagate into the transmembrane region. Notably, glycosylation reduces water permeability by narrowing the pore near the extracellular entrance, thereby lowering water occupancy and permeation frequency. These structural rearrangements are accompanied by glycosylation-induced displacements of helices 1 and 5, which alter hydrogen-bond interactions involving residues such as His180 and Arg195, components of the aromatic/arginine selectivity filter. These findings reveal how extracellular glycosylation directly modulates AQP1 channel architecture and function, suggesting a general regulatory mechanism for aquaporin family members bearing glycosylation sites in extracellular loops.

Received 10th May 2025,
Accepted 9th August 2025

DOI: 10.1039/d5cp01753j

rsc.li/pccp

Introduction

Aquaporins (AQPs) are a family of transmembrane proteins that form water channels at the plasma membrane of many cell types.[1] The crystal structures of AQPs typically reveal 7 to 9 water molecules arranged in a single file along the narrow channel pore (*e.g.*, ref. 2 and 3). A distinct feature of AQPs is their ability to facilitate selective water transport while strictly excluding protons, a property essential for maintaining osmotic balance in cells and tissues. Several mechanisms have been proposed to explain the origin of this selective water permeability, focusing on structural and electrostatic factors in the channel. One widely discussed model proposes that, as water molecules move in a single-file arrangement through the narrow pore, they undergo a characteristic reorientation at the midpoint, which disrupts proton conduction *via* the Grotthuss mechanism (*e.g.*, ref. 4 and 5). An alternative model suggests that the hydrophobic regions of the channel impose a significant desolvation penalty on protons attempting to enter, further enhancing the electrostatic barrier (*e.g.*, ref. 6). While these structural features likely contribute to proton exclusion, it is primarily the electrostatic barrier induced by key residues in the channel that plays a central role. Specifically, the conserved asparagine–proline–alanine (NPA) motifs located near the center of the pore, along with the aromatic/arginine selectivity filter near the extracellular side, generate an energetic barrier that prevents proton permeation while allowing water molecules to pass freely (*e.g.*, ref. 7 and 8). This model based on electrostatic protein environment provides a key framework for understanding how AQPs achieve both high water conductance and proton impermeability. Indeed, proton transfer from the bulk region toward the inner core of the channel is energetically uphill in AQP,[9] in contrast to the energetically downhill proton transfer observed along proton-conducting channels in photosystem II, the water-splitting enzyme.[10,11]

The APQ family, including AQP0 to AQP12, is also known to undergo asparagine-linked (*N*-linked) glycosylation, a post-translational modification where carbohydrate chains are attached to asparagine residues within specific consensus sequences, the conserved Asn–X–Ser/Thr motif, where X can be any amino acid except proline.[12] Human AQP1 is constitutively expressed in the proximal tubules of the cortex, facilitating water reabsorption. In the outer medulla, it is present in the descending thin limbs and vasa recta, where it plays a crucial role in urine concentration under varying osmotic conditions (*e.g.*, ref. 13). Human AQP1 contains two glycosylation sites,

[a] *Department of Applied Chemistry, The University of Tokyo, 7-3-1 Hongo, Bunkyo-ku, Tokyo 113-8654, Japan. E-mail: hiro@appchem.t.u-tokyo.ac.jp*
[b] *Research Center for Advanced Science and Technology, The University of Tokyo, 4-6-1 Komaba, Meguro-ku, Tokyo 153-8904, Japan. E-mail: ksaito@appchem.t.u-tokyo.ac.jp*
[c] *Department of Chemistry, Osaka University, 1-1 Machikaneyama, Toyonaka, 560-0043, Japan. E-mail: kajihara@chem.sci.osaka-u.ac.jp*

Asn42, located in the Asn42–Gln43–Thr44 motif within the extended extracellular loop connecting transmembrane helices 1 and 2 (loop 1–2), and Asn205, located in the Asn205–Phe206–Ser207 motif within the extracellular loop connecting half helix E and transmembrane helix 6 (loop E–6).[14–17] These motifs, characteristic of Asn–X–Ser/Thr sequences, suggest that AQP1 can be glycosylated at both Asn42 and Asn205 with *N*-linked glycans, forming a complex-type glycosylation pattern. Although these motifs are unique to human AQP1 and not fully conserved among the AQP family, glycosylation at Asn42 has been shown to be critical for proper glycan processing and the formation of complex glycans.[14,17] Glycosylation at AQP1 has been suggested to play a role in its stability, expression, and potentially membrane localization.[18] Glycosylation also occurs in other AQPs, although the specific glycosylation sites are not universally conserved. In human AQP2, glycosylation at Asn123 in the conserved Asn–X–Ser/Thr motif of the extracellular loop between transmembrane helices 3 and 4 plays a critical physiological role. A mutation in this motif (*e.g.*, T125M) disrupts glycosylation at Asn123, leading to recessive nephrogenic diabetes insipidus.[19,20] In human AQP10, glycosylation at Asn133 in the extracellular loop between helices 3 and 4 results in a 3–6 °C higher apparent melting temperature compared to its non-glycosylated form, indicating enhanced thermostability.[21] These examples suggest that glycosylation in the AQP family is directly linked to their structural stability and physiological functions.

Despite these findings, the specific structural and functional impacts of glycosylation on AQP1 remain unclear. Given its crucial role in water transport, it is essential to understand how glycosylation influences the protein structure and potentially the function of AQP1. In this study, we address these gaps by investigating the structural and functional consequences of glycosylation in AQP1 conducting molecular dynamics (MD) simulations of glycosylated and non-glycosylated AQP1.

Methods

Atomic coordinates and partial charges

The atomic coordinates of monomeric human AQP1 were obtained from a refined structure (PDB code: 1H6I[22]), which was derived through electron crystallographic refinement to resolve structural deviations observed in MD simulations of the original AQP1 crystal structure (PDB code: 1FQY[16]). Atomic partial charges of amino acids were adopted from the all-atom CHARMM22[23] parameter set. H atoms were generated and energetically optimized using CHARMM.[24] During the optimization of H-atom positions, all titratable groups were assigned to their most likely protonation states, with acidic residues deprotonated and basic residues protonated.

Although AQP1 physiologically assembles into tetramers, each monomer functions as an independent water channel.[25] The monomeric form has also been shown to be functional in experimental studies on tobacco aquaporin[26] and AqpZ.[27] In the present study, the monomeric form was adopted, following previous MD studies on AQP1,[28] to examine the structural and functional effects of glycosylation. This approach allows a more direct assessment of glycosylation-induced modulation, without adding the complexity of inter-subunit interactions as a starting point.

Among the two glycosylation sites, Asn42 and Asn205, Asn42 is located at the monomer–monomer interface in the tetrameric structure, whereas Asn205 is positioned outside the interface. According to theoretical analysis by Drewniak *et al.*, glycosylation at Asn42 may participate in inter-subunit interactions *via* a salt bridge with Asp131 in the adjacent monomer in two of the four subunits within the tetramer.[29] Therefore, glycosylation effects observed in the monomeric AQP1 may partially differ from those in the full tetrameric assembly. Nonetheless, the present monomer-based analysis allows us to isolate and characterize the direct, intrinsic structural effects of glycosylation on the AQP1 subunit.

It should also be noted that, for experimental validation of the present study, monomeric AQP1 will be prepared by introducing interface mutations to prevent tetramerization and expressing the protein on the cell surface. This strategy enables site-specific enzymatic glycan modification (*e.g.*, sialidase treatment to remove terminal sialic acid), simplifying the preparation of well-defined glycoforms corresponding to those used in the present simulations. Thus, adopting the monomeric form is consistent with both the computational model and planned experimental approaches.

N-Linked glycans, which are composed of neutral monosaccharide residues and thus carry no net charge under physiological conditions, were modeled at the glycosylation sites Asn42 and Asn205, both of which are part of the Asn–X–Ser/Thr motif, where X can be any amino acid except proline.[12] The asparagine side chain is glycosylated with a reducing terminal *N*-acetylglucosamine (GlcNAc). The attached glycan, from the reducing terminal to the non-reducing terminal, consists of two GlcNAc residues linked by β(1 → 4), followed by a branched mannose core linked to GlcNAc *via* β(1 → 4) form. The branched mannose core is linked to two mannose (Man) residues linked by α(1 → 3) and α(1 → 6). Both branches of the mannose core are extended by β(1 → 2)-linked GlcNAc residues, which are further capped by β(1 → 4)-linked galactose (Gal) residues (Fig. S3). This glycan represents a common complex-type *N*-linked glycosylation pattern, characterized by a branched mannose core and terminal GlcNAc and Gal residues, frequently observed in mammalian glycoproteins,[12] and experimentally identified at Asn42 in AQP1.[14,17]

Protonation pattern

The protonation pattern of the titratable residues was determined by solving the linear Poisson–Boltzmann equation using the MEAD program.[30] All calculations were conducted at 300 K, pH 7.0, and an ionic strength of 100 mM, with dielectric constants of 4 for the protein interior and 80 for bulk water. To calculate the pK_a values of titratable sites in the protein, the calculated pK_a difference between the protein site and the reference system was added to the known reference pK_a value

(*e.g.*, 4.0 for Asp[31]). Experimentally measured pK_a values used as references were 12.0 for Arg, 4.0 for Asp, 9.5 for Cys, 4.4 for Glu, 10.4 for Lys, 9.6 for Tyr,[31] and 7.0 and 6.6 for the N_ε and N_δ atoms of His, respectively.[32–34] Protonation patterns were sampled using a Monte Carlo method with Karlsberg.[35] The linear Poisson–Boltzmann equation was solved through a three-step grid-focusing procedure at resolutions of 2.5 Å, 1.0 Å, and 0.3 Å. Monte Carlo sampling provided the probabilities of the protonated and deprotonated states for each titratable site. The resulting protonation patterns were subsequently used in MD simulations: His204 was doubly-protonated and all other titratable side chains were in their standard protonation states (*i.e.*, singly protonated for histidine residues, protonated for other basic residues, and deprotonated for acidic residues).

MD simulations

The AQP1 assembly was embedded in a lipid bilayer consisting of 387 1-palmitoyl-2-oleyl-*sn*-glycero-3-phosphocholine (POPC) molecules using CHARMM-GUI[36] and soaked in 31 096–34 314 TIP3P water models, and 6 chloride ions were added to neutralize the system using VMD plugins.[37] After structural optimization with position restraints on the heavy atoms of the AQP1 assembly, the system was heated from 0.1 to 300 K over 5.5 ps with a time step of 0.1 fs, equilibrated at 300 K for1 ns with a time step of 0.5 fs, and annealed from 300 to 0 K over 5.5 ps with a time step of 0.1 fs. The positional restraints on the heavy atoms of the side-chains were released, and the same procedure was repeated. The positional restraints on any atoms were released, and the system was heated from 0.1 to 300 K over 5.5 ps with a time step of 0.1 fs and equilibrated at300 K for 1 ns with a time step of 0.5 fs. The system was equilibrated at 300 K for 225 ns with a time step of 1.5 fs. Five independent 225-ns simulations were performed for both glycosylated and non-glycosylated AQP1. All MD simulations were conducted with the CHARMM22 force field parameter set[23] using the MD engine NAMD version2.15.[38] For MD simulations with a time step of 1.5 fs, the SHAKE algorithm for hydrogen constraints was employed.[39] For temperature and pressure control, the Langevin thermostat and piston were used.[40,41] Atomic coordinates generated performing MD simulations are provided in SI (SI coordinates).

Results and discussion

Enhanced disorder of channel water molecules upon glycosylation

Although water molecules are invisible in the reported human AQP1 crystal structures[16,22,42] (Fig. 1a), MD simulations indicate the presence of water molecules along the channel pore (Fig. 2). The positions of these water molecules are essentially consistent with those identified in the bovine AQP1 structure, which assigned seven water molecules in the channel pore[43] (Fig. 1b).

While the number of surface water (*i.e.*, hydrated water) molecules on the intracellular surface remains unchanged between glycosylated and non-glycosylated AQP1 proteins (~90 water molecules), glycosylated AQP1 exhibits approximately 70 more H-bound water molecules on the extracellular surface than non-glycosylated AQP1 (Fig. 2). This observation

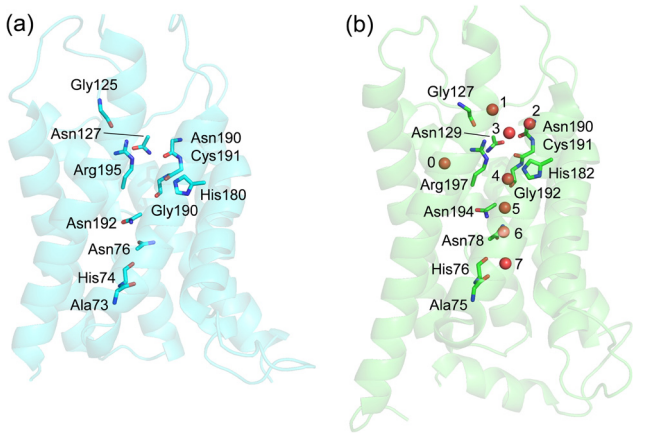

Fig. 1 Overview of mammalian APQ1 structures. (a) Human AQP1 (PDB ID: 1H6I). (b) Bovine AQP1 (PDB ID: 1J4N). Red spheres indicate water molecules in the transmembrane region. Water molecules 1 to 7 are located along the water channel, and water molecule 0 is beside the channel, near the side chain of Thr111 (at a distance of 2.8 Å) and the backbone oxygen atom of Arg197 (2.4 Å) adjacent to the channel. No water molecules are assigned in the human AQP1 structure.

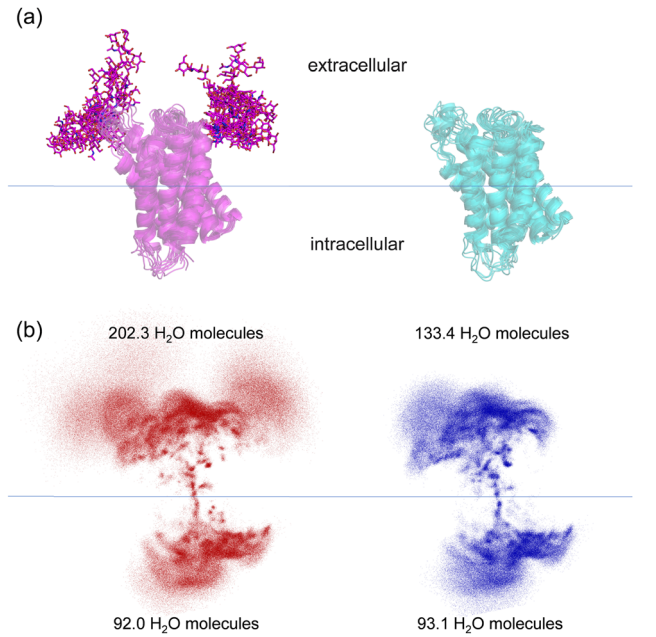

Fig. 2 Overview of structural fluctuations and water molecule distributions during molecular dynamics simulations. (a) Structural fluctuations, including glycans. (b) Water molecule distributions within 3.2 Å of the protein and glycan surfaces. Left panels show glycosylated AQP1, and right panels show non-glycosylated AQP1. Red and blue dots represent accumulated positions of water molecules. Blue horizontal lines indicate the midplane of the transmembrane region, analyzed using the PPM server.[44] Numerical values represent the average number of water molecules on the extracellular and intracellular sides. The configurations and water distributions were accumulated over five 225-ns MD trajectories. See Fig. S1 for water distributions in individual trajectories.

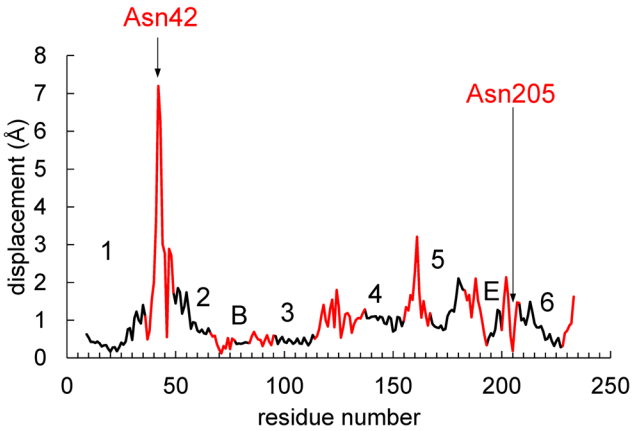

Fig. 3 Displacements of Cα atoms between glycosylated and non-glycosylated AQP1 structures. Displacements are averaged over five 225-ns MD trajectories. Black and red lines represent the displacement of residues in helix and connecting (*e.g.*, loop) regions, respectively. Labels 1–6, B, and E indicate the six transmembrane helices and two half-helices, respectively. The positions of the glycosylation sites Asn42 and Asn205 are indicated.

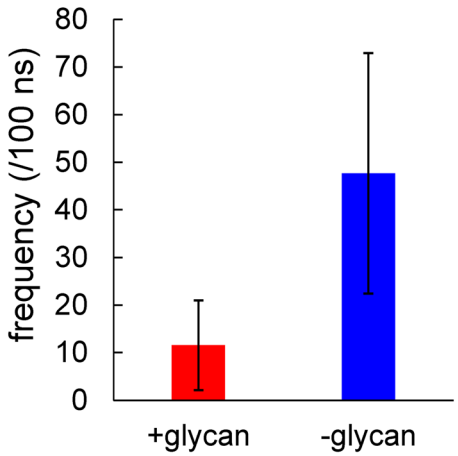

Fig. 5 Frequency of water molecule permeation events in the channel in the time region of 37.5–150 ns, averaged over five MD trajectories. Error bars represent standard deviations among trajectories. See Fig. S2 for permeation details in individual trajectories.

suggests that glycosylation substantially increases the hydration surface, primarily as by extending the extracellular protein bulk surface.

To address this, below structural differences and fluctuations between glycosylated and non-glycosylated AQP1 proteins are analyzed.

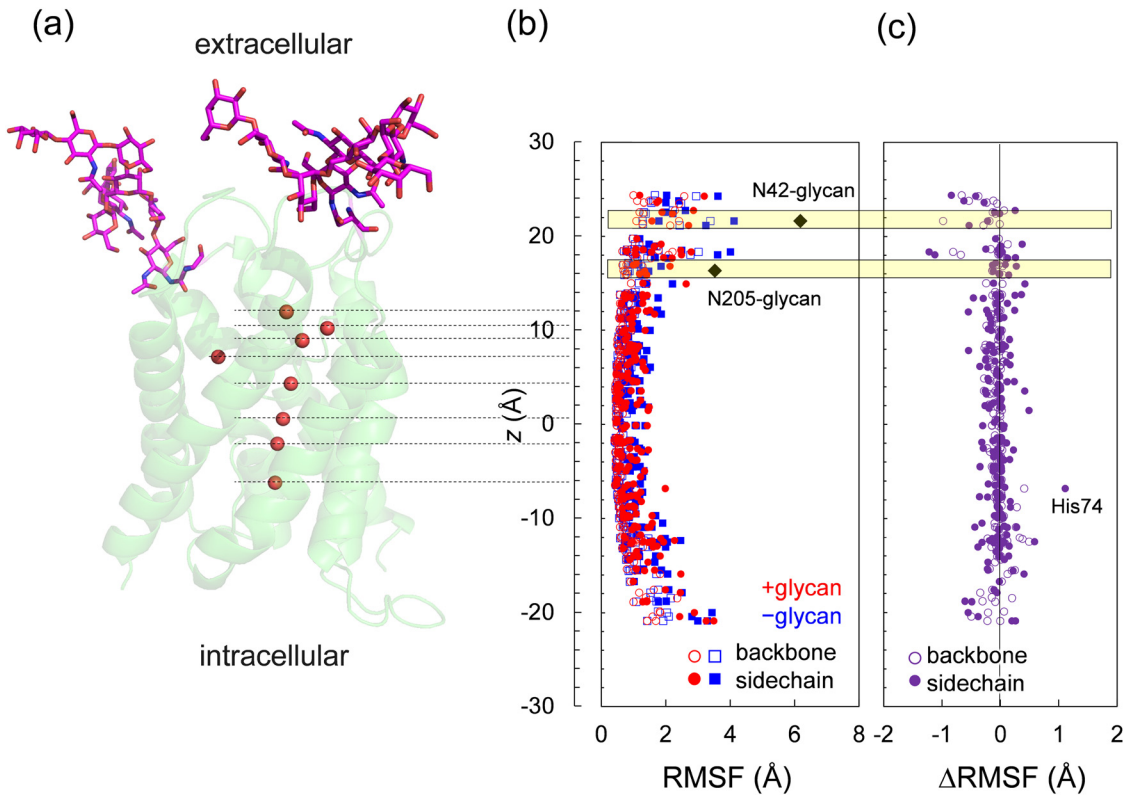

Fig. 4 Comparison of structural fluctuations along the transmembrane axis, *z*, between glycosylated and non-glycosylated AQP1 structures in equilibrium. (a) Overall shape of the glycosylated AQP1 structure. (b) Root mean square fluctuations (RMSF) for glycosylated (red) and non-glycosylated (blue) AQP1 structures (Å). (c) RMSF differences (non-glycosylated AQP1 minus glycosylated AQP1) between glycosylated AQP1 and non-glycosylated AQP1 (Å). Open circles and squares represent values for backbone regions, whereas closed circles and squares represent values for side chains. Black closed squares represent values for glycans. Yellow bands highlight regions near glycan-linked asparagine residues, Asn42 and Asn205. The values were averaged over five 225-ns MD trajectories.

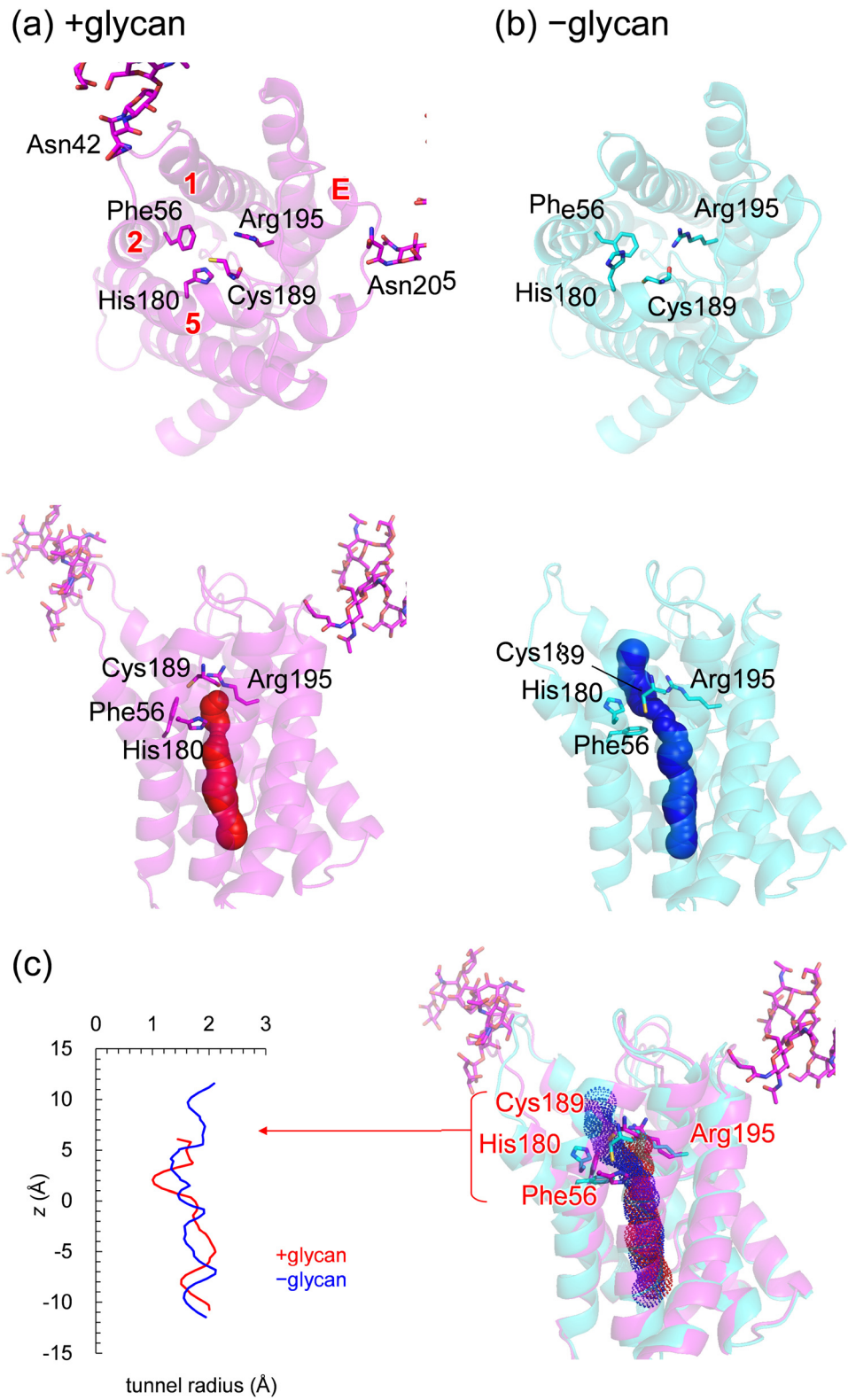

Fig. 6 Channel shape comparison between glycosylated and non-glycosylated AQP1. (a) Averaged structure of glycosylated AQP1 (magenta). (b) Averaged structure of non-glycosylated AQP1 (cyan). Upper panels: top views from the extracellular side. Lower panels: side views with channel pathways. (c) Channel radius along the transmembrane axis, z (Å), comparing glycosylated (magenta) and non-glycosylated (cyan) AQP1 structures. Structures were averaged over five MD trajectories in the time region of 37.5–150 ns, followed by geometry optimizations of amino-acid side chains. The peak for glycosylated AQP1 in the left panel corresponds to the inner surface formed by Phe56, His180, Cys189, and Arg195. Labels 1,2, 5, and E indicate helices.

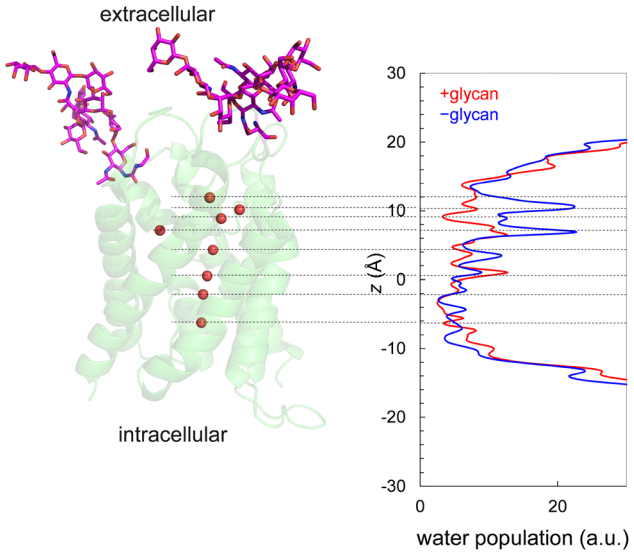

Fig. 7 Population of water molecules in the channel.

Reduced fluctuations in glycosylated AQP1

Structural comparisons reveal that the most significant structural displacement upon glycosylation occurs in the extended extracellular loop 1–2 (Tyr37 to Asp48), which contains Asn42, the glycan-linked residue (Fig. 3). In contrast, the second glycosylation site at Asn205, located in the shorter extracellular loop between Val201 and Ser207 (loop E–6), does not exhibit significant structural displacement, likely due to the loop's shorter length and relatively rigid conformation.

In addition, the extended loop 1–2, containing Asn42, exhibits reduced backbone fluctuations after glycosylation (Fig. 4), consistent with the widely accepted view that glycosylation enhances protein stability and reduces protein flexibility.[45] Thus, glycosylation does not induce structural fluctuations but instead facilitates energetically favorable structural changes in the otherwise fluctuating extended loop 1–2, resulting in a more stabilized conformation.

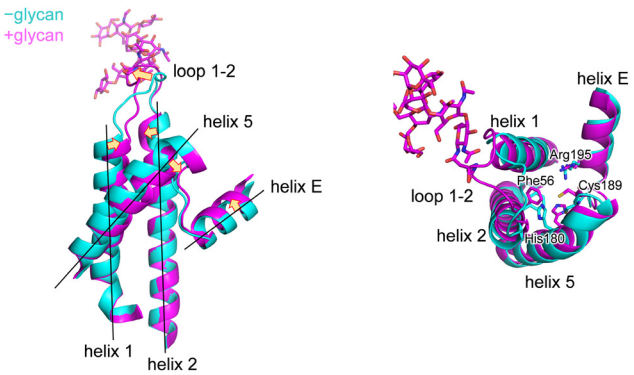

Fig. 8 Glycosylation-induced structural rearrangement in AQP1. Left panel: side view. Right panel: top view from the extracellular side. Arrows indicate the directions of structural changes upon glycosylation. The structures were averaged over five MD trajectories (37.5–150 ns), followed by geometry optimizations of amino-acid side chains.

Table 1 Changes in the H-bond pattern upon glycosylation (difference > 30%). Values represent averages over five MD trajectories in the time region of 37.5–150 ns. CO: backbone carbonyl group. NH: backbone NH group

Donor		Acceptor		H-bond formation ratio	
Residue	Region	Residue	Region	+Glycan (%)	−Glycan (%)
Ile27CO	Helix 1	Ser31	Helix 1	88.5	31.5
Ser53	Helix 2	His180	Helix 5	0.0	50.4
Ile106CO	Helix 3	Ala110NH	Helix 3	35.0	67.3
Leu112CO	Helix 3	Thr116	Loop 3–4	67.4	35.8
Asn127	Loop 3–4	Arg195	Half-helix E	48.0	4.7
Glu142	Helix 4	Thr187	Loop 5–E	96.8	38.3
Asp158	Loop 4–5	Arg160	Loop 4–5	62.8	16.9
Ala171CO	Helix 5	Ser175	Helix 5	56.8	24.5
Gly198	Half-helix E	Thr109	Half-helix E	52.3	1.9
Ser199CO	Half-helix E	Thr203NH	Loop E–6	32.1	65.3
Ser199CO	Half-helix E	Thr203	Loop E–6	54.9	84.7
His209	Helix 6	Trp213NH	Helix 6	19.0	61.8
Leu231CO	Loop 6–C	Arg160	Loop 4–5	47.5	0.3

Although the His74 side chain is oriented away from the channel pore, it exhibits increased fluctuations upon glycosylation (Fig. 4c). This observation suggests that glycosylation affects not only water molecules within the channel pore (Fig. 2b, left) but also those in adjacent regions, leading to a broader disruption of water organization and enhanced fluctuation of His74.

Mechanism for glycosylation-induced structural changes in the channel pore

Remarkably, the present results indicate that glycosylation reduces the water permeability of AQP1. The frequency of water permeation events is significantly higher in non-glycosylated AQP1 than in glycosylated AQP1 (Fig. 5 and Fig. S2). In glycosylated AQP1 structure, the extracellular side of the channel was partially occluded (Fig. 6a), in contrast to the more open configuration observed in the non-glycosylated form (Fig. 6b). This occlusion narrows the pore radius near the extracellular entrance (Fig. 6c), thereby limiting water access to the inner channel region. Apart from this constriction at the extracellular side, the overall channel radius profiles along the transmembrane axis show no substantial differences between glycosylated and non-glycosylated AQP1 (Fig. 6b and c).

Consistent with this narrower extracellular entrance, the average number of water molecules in this region is significantly lower in glycosylated AQP1 than in non-glycosylated AQP1 (Fig. 7). This reduction in local water density explains why the frequency of water permeation events becomes lower upon glycosylation.

As the origin of these structural changes, glycosylation induces displacements of helices 1 and 5 (Fig. 8), which lead to altered hydrogen-bonding patterns involving key residues such as His180 (helix 5) and Arg195 (half-helix E) (Table 1). These residues have been implicated in forming the "aromatic/

arginine selectivity filter'' (*e.g.*, ref. 1, 29 and 46–48). Consequently, glycosylation at the extended loop can directly modify the geometry of the channel pore.

This mechanism is also consistent with previous findings that interactions between an AQP1 blocker, tetraethylammonium, and the extended loop 1–2, where the glycosylation site is situated, account for the loss of tetraethylammonium inhibition in the N42A AQP1 mutant.[49] Together, these results provide a molecular framework for understanding how glycosylation modulates the structure and function of AQP1.

Conclusions

The structural and functional consequences of glycosylation in AQP1 were investigated using MD simulations. Glycosylation at Asn42 significantly stabilizes the extended extracellular loop 1–2 by suppressing its backbone fluctuations (Fig. 4). This stabilization results in a pronounced stretching of loop 1–2, driven by the formation of a structured hydration shell surrounding the glycan. The glycan-associated hydration shell appears to effectively decouple the glycan from the protein surface, triggering conformational changes that propagate into the transmembrane region. Glycosylation reduces water permeability through AQP1. The frequency of water permeation events is significantly lower in glycosylated AQP1 than in the non-glycosylated form (Fig. 5 and Fig. S2). This reduction is attributable to a narrowing of the pore radius near the extracellular entrance, where the loop 1–2 undergoes structural rearrangement upon glycosylation (Fig. 6). In contrast, no substantial differences in pore radius are observed along the other region of the channel. Consistent with the narrowing, the average water density in the extracellular portion of the channel is significantly reduced in glycosylated AQP1 (Fig. 7), limiting access to the channel interior. These structural rearrangements originate from glycosylation-induced displacements in helices 1 and 5 lead to modified H-bond interactions involving residues such as His180 and Arg195, which are part of the aromatic/arginine selectivity filter (Table 1). These findings demonstrate that glycosylation not only modulates protein conformation but also alters water transport properties by changing the geometry and hydration environment adjacent to the channel pore.

The observed structural modulations, triggered by the formation of a heavily hydrated shell surrounding the glycan attached to the conserved Asn–X–Ser/Thr motif and the subsequent stretching of the extracellular loop away from the protein, may represent a common mode of functional modulation in the AQP family, provided the glycosylation site is located in an extracellular loop.

Conflicts of interest

There are no conflicts to declare.

Data availability

The data supporting this article have been included as part of the SI.

Supplementary information available: Water molecule distributions for each of the five individual MD trajectories (Fig. S1); trajectories along the *z*-axis of oxygen atoms of water molecules that permeate the channel (Fig. S2); structure of the *N*-linked glycan (Fig. S3); atomic coordinates of the averaged structure of glycosylated AQP1. See DOI: **https://doi.org/10.1039/d5cp01753j**

Acknowledgements

This research was supported by JSPS KAKENHI (JP23H04963 and JP24K01986 to K.S.; JP23H02444 to H.I.) and Interdisciplinary Computational Science Program in CCS, University of Tsukuba.

References

1 Y. Fujiyoshi, K. Mitsuoka, B. L. de Groot, A. Philippsen, H. Grubmüller, P. Agre and A. Engel, *Curr. Opin. Struct. Biol.*, 2002, **12**, 509–515.
2 D. Kozono, M. Yasui, L. S. King and P. Agre, *J. Clin. Invest.*, 2002, **109**, 1395–1399.
3 J. D. Ho, R. Yeh, A. Sandstrom, I. Chorny, W. E. Harries, R. A. Robbins, L. J. Miercke and R. M. Stroud, *Proc. Natl. Acad. Sci. U. S. A.*, 2009, **106**, 7437–7442.
4 E. Tajkhorshid, P. Nollert, M. Jensen, L. J. Miercke, J. O'Connell, R. M. Stroud and K. Schulten, *Science*, 2002, **296**, 525–530.
5 M. Jensen, E. Tajkhorshid and K. Schulten, *Biophys. J.*, 2003, **85**, 2884–2899.
6 B. L. de Groot and H. Grubmüller, *Science*, 2001, **294**, 2353–2357.
7 A. Burykin and A. Warshel, *FEBS Lett.*, 2004, **570**, 41–46.
8 A. Warshel, *Proc. Natl. Acad. Sci. U. S. A.*, 2005, **102**, 1813–1814.
9 N. Sakashita, H. Ishikita and K. Saito, *Phys. Chem. Chem. Phys.*, 2020, **22**, 15831–15841.
10 K. Saito, A. W. Rutherford and H. Ishikita, *Nat. Commun.*, 2015, **6**, 8488.
11 T. Takaoka, N. Sakashita, K. Saito and H. Ishikita, *J. Phys. Chem. Lett.*, 2016, **7**, 1925–1932.
12 R. Kornfeld and S. Kornfeld, *Annu. Rev. Biochem.*, 1985, **54**, 631–664.
13 S. Nielsen, T. Pallone, B. L. Smith, E. I. Christensen, P. Agre and A. B. Maunsbach, *Am. J. Physiol.*, 1995, **268**, F1023–1037.
14 G. M. Preston, J. S. Jung, W. B. Guggino and P. Agre, *J. Biol. Chem.*, 1994, **269**, 1668–1673.
15 B. L. Smith, G. M. Preston, F. A. Spring, D. J. Anstee and P. Agre, *J. Clin. Invest.*, 1994, **94**, 1043–1049.
16 K. Murata, K. Mitsuoka, T. Hirai, T. Walz, P. Agre, J. B. Heymann, A. Engel and Y. Fujiyoshi, *Nature*, 2000, **407**, 599–605.
17 F. Magni, C. Chinello, F. Raimondo, P. Mocarelli, M. G. Kienle and M. Pitto, *Expert Rev. Proteomics*, 2008, **5**, 29–43.

18 P. D. Cabral and M. Herrera, *Am. J. Physiol. Renal. Physiol.*, 2012, **303**, F621–629.
19 K. Goji, M. Kuwahara, Y. Gu, M. Matsuo, F. Marumo and S. Sasaki, *J. Clin. Endocrinol. Metab.*, 1998, **83**, 3205–3209.
20 G. Hendriks, M. Koudijs, B. W. M. van Balkom, V. Oorschot, J. Klumperman, P. M. T. Deen and P. van der Sluijs, *J. Biol. Chem.*, 2004, **279**, 2975–2983.
21 F. Öberg, J. Sjöhamn, G. Fischer, A. Moberg, A. Pedersen, R. Neutze and K. Hedfalk, *J. Biol. Chem.*, 2011, **286**, 31915–31923.
22 B. L. de Groot, A. Engel and H. Grubmüller, *FEBS Lett.*, 2001, **504**, 206–211.
23 A. D. MacKerell, Jr., D. Bashford, R. L. Bellott, R. L. Dunbrack, Jr., J. D. Evanseck, M. J. Field, S. Fischer, J. Gao, H. Guo, S. Ha, D. Joseph-McCarthy, L. Kuchnir, K. Kuczera, F. T. K. Lau, C. Mattos, S. Michnick, T. Ngo, D. T. Nguyen, B. Prodhom, W. E. Reiher, I. I. I. B. Roux, M. Schlenkrich, J. C. Smith, R. Stote, J. Straub, M. Watanabe, J. Wiorkiewicz-Kuczera, D. Yin and M. Karplus, *J. Phys. Chem. B*, 1998, **102**, 3586–3616.
24 B. R. Brooks, R. E. Bruccoleri, B. D. Olafson, D. J. States, S. Swaminathan and M. Karplus, *J. Comput. Chem.*, 1983, **4**, 187–217.
25 L. B. Shi, W. R. Skach and A. S. Verkman, *J. Biol. Chem.*, 1994, **269**, 10417–10422.
26 B. Otto, N. Uehlein, S. Sdorra, M. Fischer, M. Ayaz, X. Belastegui-Macadam, M. Heckwolf, M. Lachnit, N. Pede, N. Priem, A. Reinhard, S. Siegfart, M. Urban and R. Kaldenhoff, *J. Biol. Chem.*, 2010, **285**, 31253–31260.
27 V. Schmidt and J. N. Sturgis, *ACS Omega*, 2017, **2**, 3017–3027.
28 N. Smolin, B. Li, D. A. Beck and V. Daggett, *Biophys. J.*, 2008, **95**, 1089–1098.
29 P. Drewniak, P. Xiao, V. Ladizhansky, A.-N. Bondar and L. S. Brown, *Biophys. J.*, 2024, **123**, 4285–4303.
30 D. Bashford and M. Karplus, *Biochemistry*, 1990, **29**, 10219–10225.
31 Y. Nozaki and C. Tanford, *J. Am. Chem. Soc.*, 1967, **89**, 736–742.
32 M. Tanokura, *J. Biochem.*, 1983, **94**, 51–62.
33 M. Tanokura, *Biochim. Biophys. Acta*, 1983, **742**, 576–585.
34 M. Tanokura, *Biochim. Biophys. Acta*, 1983, **742**, 586–596.
35 B. Rabenstein and E.-W. Knapp, *Biophys. J.*, 2001, **80**, 1141–1150.
36 S. Jo, T. Kim, V. G. Iyer and W. Im, *J. Comput. Chem.*, 2008, **29**, 1859–1865.
37 W. Humphrey, A. Dalke and K. Schulten, *J. Mol. Graphics*, 1996, **14**, 33–38.
38 J. C. Phillips, R. Braun, W. Wang, J. Gumbart, E. Tajkhorshid, E. Villa, C. Chipot, R. D. Skeel, L. Kale and K. Schulten, *J. Comput. Chem.*, 2005, **26**, 1781–1802.
39 J.-P. Ryckaert, G. Ciccotti and H. J. C. Berendsen, *J. Comput. Phys.*, 1977, **23**, 327–341.
40 R. Kubo, M. Toda and N. Hashitsume, *Statistical Physics II*, Springer, Berlin, Heidelberg, 1991.
41 S. E. Feller, Y. H. Zhang, R. W. Pastor and B. R. Brooks, *J. Chem. Phys.*, 1995, **103**, 4613–4621.
42 G. Ren, V. S. Reddy, A. Cheng, P. Melnyk and A. K. Mitra, *Proc. Natl. Acad. Sci. U. S. A.*, 2001, **98**, 1398–1403.
43 H. Sui, B.-G. Han, J. K. Lee, P. Walian and B. K. Jap, *Nature*, 2001, **414**, 872–878.
44 M. A. Lomize, I. D. Pogozheva, H. Joo, H. I. Mosberg and A. L. Lomize, *Nucleic Acids Res.*, 2012, **40**, D370–376.
45 D. Shental-Bechor and Y. Levy, *Curr. Opin. Struct. Biol.*, 2009, **19**, 524–533.
46 E. Beitz, B. Wu, L. M. Holm, J. E. Schultz and T. Zeuthen, *Proc. Natl. Acad. Sci. U. S. A.*, 2006, **103**, 269–274.
47 D. Seeliger, C. Zapater, D. Krenc, R. Haddoub, S. Flitsch, E. Beitz, J. Cerdà and B. L. de Groot, *ACS Chem. Biol.*, 2013, **8**, 249–256.
48 D. A. Dingwell, L. S. Brown and V. Ladizhansky, *J. Phys. Chem. B*, 2019, **123**, 7700–7710.
49 F. J. Detmers, B. L. de Groot, E. M. Müller, A. Hinton, I. B. Konings, M. Sze, S. L. Flitsch, H. Grubmüller and P. M. Deen, *J. Biol. Chem.*, 2006, **281**, 14207–14214.

